Journal of Visualization, Vol. 4, No. 2 (2001) 197-207

Computational Study of Influences of a Seam Line of a Ball for Baseball on Flows

Himeno, R.*

* RIKEN (The Institute of the Physical and Chemical Research), 2-1, Hirosawa, Wako, Saitama, 351-0198 Japan.

Received 5 February, 2001
Revised 19 February, 2001

***Abstract*:** Flows around a ball used in baseball games are calculated using third-order upwind-difference method with various seam positions determined by two rotation angles. Those are four-seam rotation with an angle: *a* and two-seam rotation with an angle: *b*. The computed results of the four-seam rotation are compared with experimental data measured in a wind tunnel and computed drag coefficients qualitatively agree well with experiments. However, lift coefficients do not agree well. The computed results and geometrical symmetry suggest that a supporting rod in the wind tunnel would have strong influence on the accuracy of the measurement.

Flow changes in two-seam rotation are also simulated. It is found that the lowest drag force is observed at *b*=90 and that the value is less than half of the largest drag force at *a*=30 and 60 degrees. The largest lift force is observed at *b*=20 degree. In this case, a projection of the seam line on the top causes a large separation while smooth surface without the seam at the bottom dose not separate the flow. A pair of longitudinal vortices are found in the wake, which make wake slant and generate large lift force.

***Keywords*:** baseball, CFD, wake, aerodynamic coefficient, longitudinal vortex.

1. Introduction

A ball used in baseball games has a peculiar seam line on its surface. The seam line makes a groove and rib, whose height is about 1 mm and very small to the diameter of the ball: about 70 mm. It is well known that the unique curved seam line gives large influence on flows around the ball. Tani(1950) reported that the seam line works as surface roughness on a sphere and makes Magnus force larger than that of a ball without seam. Watts and Sawyer(1975) reported that asymmetric aerodynamic force acts on the ball and changes its direction when the ball is slowly rotating, which is the reason why knuckle ball has curious trajectory. Mizota et al.(1995) performed wind tunnel experiments and measured aerodynamic forces of the ball at various seam positions. They reported the seam makes the boundary layer turbulent and the asymmetric position of the seam lets wake asymmetric, resulting in asymmetric aerodynamic force. However, balls were supported by rods in all these wind tunnel experiments and the influence of the rod is not clear. Mizota et al.(1995) showed the asymmetric position of the seam makes asymmetric wake but they only measured the influence in two-dimensional section. Three-dimensional structure of the wake is not clear now.

Recently, CFD has been rapidly developed and is widely applied now. We calculated flows around the ball with the seam line but no rotation. In this paper, the computed results will be shown comparing experimental results with the same conditions by Mizota et al. (1995) and the accuracy of both computation and experiments will be discussed. Three dimensional wake structure of the ball will be also investigated here.

2. Computation Method

It is believed that the fastest ball recorded in baseball games was pitched by Nolan Ryan and that its speed was more than 45 m/s (162 km/h). Therefore the flow around the ball is incompressible. Usually, ball speed in baseball games is in between 30 m/s (108 km/h) and 45 m/s (162 km/h). Reynolds number based on the ball diameter d:0.0715 m is in between 1.3×10^5 and 2.1×10^5. Flow fields would consist of laminar and turbulent regions. In this paper, the whole flow field is simulated by using third-order upwind-difference scheme without any turbulence model. This approach was successfully applied to a turbulent inner flow (Kawamura and Kuwahara, 1985) and is regarded as a quasi-DNS.

2.1 Basic Equations

Basic equations are unsteady incompressible Navier-Stokes equations and the equation of continuity. These equations are expressed on a coordinate system fixed on the ball moving with the velocity $\boldsymbol{v}_0$ through stationary fluid as follows.

$$\nabla\cdot\boldsymbol{v}=0, \tag{1}$$

$$\frac{\partial\boldsymbol{v}}{\partial t}+\left\{(\boldsymbol{v}-\boldsymbol{v}_0)\cdot\nabla\right\}\boldsymbol{v}=-\nabla p+\frac{1}{Re}D\boldsymbol{v} \tag{2}$$

where $\boldsymbol{v}$ is flow velocity, p is pressure and Re is Reynolds number. All values are non-dimensional ones.

2.2 MAC Based Scheme

In order to couple the equation of continuity and the Navier-Stokes equation, MAC method (Roache, 1976) is used here. Poisson equation for pressure in high Reynolds number regime is as follows.

$$Dp=-\nabla\cdot\left\{(\boldsymbol{v}-\boldsymbol{v}_0)\cdot\nabla\right\}\boldsymbol{v}-\frac{\partial D}{\partial t} \tag{3}$$

where $D=\nabla\cdot\boldsymbol{v}$. When the second term of the right hand side of this equation is expressed by a finite difference approximation, the next equation is obtained.

$$Dp=-\nabla\cdot\left\{(\boldsymbol{v}-\boldsymbol{v}_0)\cdot\nabla\right\}\boldsymbol{v}-\frac{D^{n+1}-D^n}{Dt} \tag{4}$$

where superscript n denotes the n-th time step and Dt is a time increment. Although the second term of the right hand side of this equation is zero due to the equation of continuity, D^n is not omitted so that any error in satisfying the equation of continuity at the present time step can be compensated as follows;

$$Dp=-\nabla\cdot\left\{(\boldsymbol{v}-\boldsymbol{v}_0)\cdot\nabla\right\}\boldsymbol{v}+\frac{D^n}{Dt} \tag{5}$$

The equation of continuity is not directly satisfied but implicitly satisfied. This derivation is based on a MAC method, which may cause the error in the flow quantity in the case of internal flows but may not cause significant errors in the case of external flows.

2.3 Third-order Upwind-difference Scheme

Equations (2) and (5) are transformed into a generalized coordinate system and discritized. A first-order Euler implicit method is used for time derivatives, a third-order upwind-difference scheme (Kawamura et al., 1986) for convective terms, and second-order central-difference for the other spatial derivative terms. This scheme is applied to various three-dimensional high Reynolds number flows and shows very good results (Kawamura and Kuwahara, 1985; Himeno et al., 1990; Ono et al., 1992).

The third-order upwind-difference scheme is as follows.

$$\begin{aligned}u\frac{\partial u}{\partial x}\bigg|_{x=x_i}&=\frac{u_i}{12\,Dx}\left\{-u_{i+2}+8(u_{i+1}-u_{i-1})-u_{i-2}\right\}\\&\quad+\frac{|u_i|}{12\,Dx}(u_{i+2}-4u_{i+1}+6u_i-4u_{i-1}+u_{i-2})\end{aligned} \tag{6}$$

where subscript i denotes i-th grid number, u is velocity component in x-direction and Dx is a finite difference increment in x-direction.

3. Grid System

The simplest grid system may be an O-type system which has a singular axis like the longitude and latitude system on the globe. However, this causes unnecessary grid concentration near the axis. Figure 1 shows the grid system used in the computation. Positions and heights of the seam line are obtained by measuring an official ball for a baseball game. Grid lines near the seam line are generated to be aligned along the seam line. Two kinds of grid system are used in the computation, a) coarse grid system with 169×92×101, about 1.6 million grid points and b) fine grid system with 337×181×101, about 6.2 million grid points, which uses four times finer grids of the coarse grids in each grid plane parallel to the ball surface.

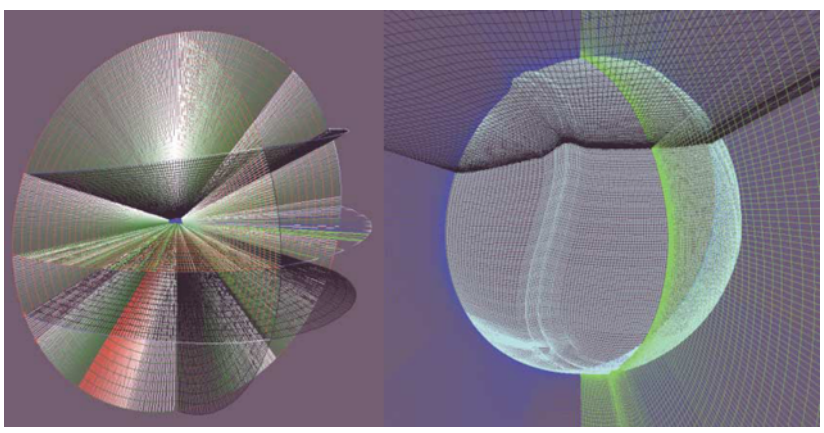

Fig. 1. Fine grid system (337×181×101 grid points).

4. Shape of the Seam on the Ball

In all the computations, the ball has no angular velocity but has some angles in two kinds of axes of the rotation. Before presenting the results, changes of the seam in the two kinds of rotation are shown here to see its geometrical symmetry. "Two-seam rotation" and "four-seam rotation" are defined as the rotation around the Z axis and the X-axis in Fig. 2 respectively. As Fig. 3 shows, the seam appears four times when the ball turns around in a-direction while the seam appears two times in b-direction. Geometrical symmetry of the seam shape is very important to investigate the influence of the seam line on the flow. Figures 4 and 5 show seam line shapes during the two kinds of rotations.

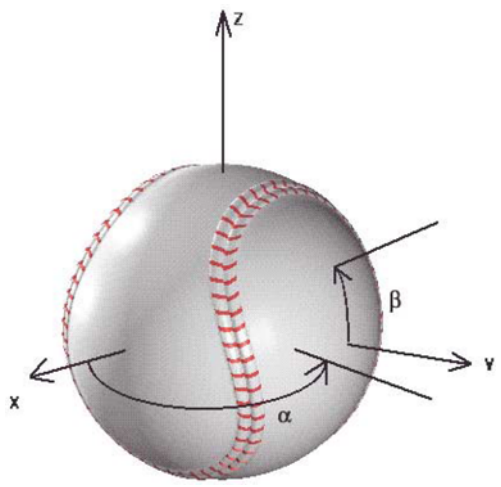

Fig. 2. Definition of coordinates and angle a, b.

(a) four-seam rotation (b) two-seam rotation

Fig. 3. Four-seam and two-seam rotations.

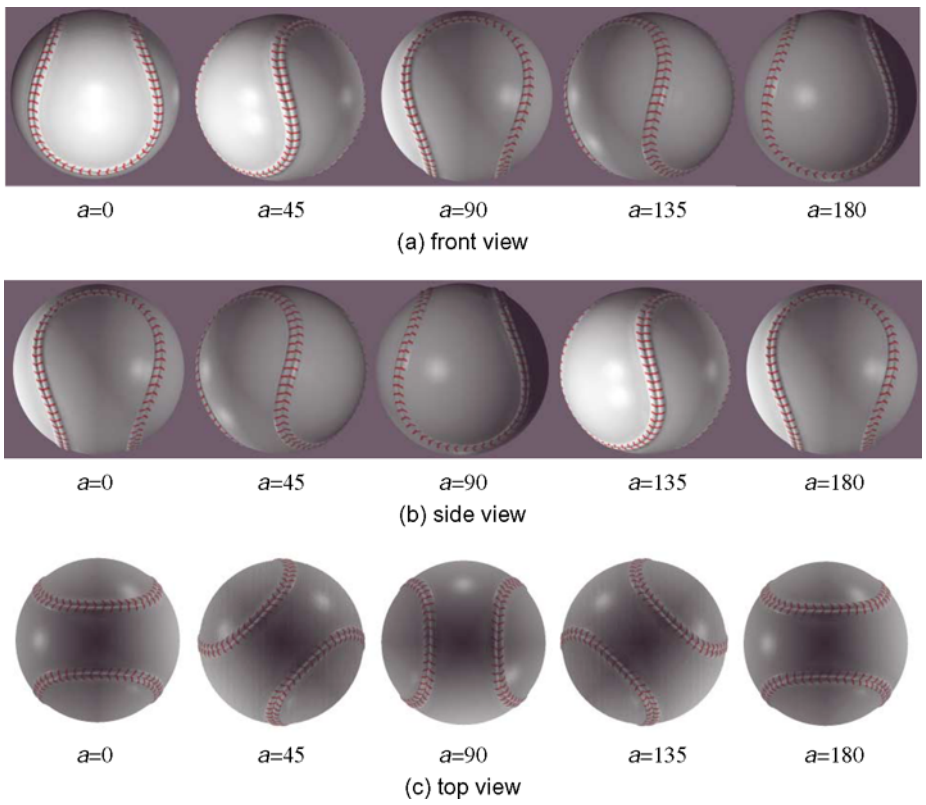

Fig. 4. Shape change of the seam (four-seam rotation).

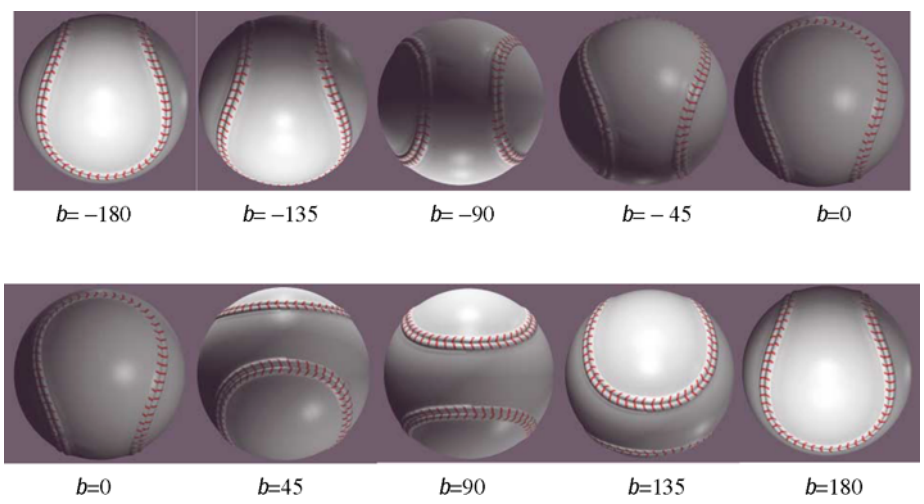

Fig. 5. Shape change of the seam (two-seam rotation, front view).

In the case of four-seam rotation, the shape change has an apparent period of *a*:180 degrees. Watching Fig. 4 carefully, it is found that the shape at *a*=90 degrees is the inverted shape at *a*=0 or 180 degrees and that the shape at *a*=135 degrees is the reversed shape at *a*=45 degrees. To get the variation of aerodynamic forces in this rotation, it is not necessary to compute flows from *a*=0 degree to 360 degrees but it is sufficient to compute flows only from *a*=0 to 45 degrees for the sake of these geometrical symmetries. However, to see the symmetry effect not only the cases of *a*=0 to 45 degrees but also the cases of *a*=45 to 90 degrees are calculated.

In the case of the two-seam rotation, the shape change has a period of *b*:360 degrees. However, watching Fig. 5 carefully, it is found that the shape at *b*=180 and −180 degrees is the inverted shape at *b*=0 degree, and that the shape at *b*=135 degrees is also the inverted shape at *a*=45 degrees. Similarly, it is found that the shape at *b*=−135 degree is the inverted shape at *b*=−45 degrees. To get variation of aerodynamic forces in this rotation, it is sufficient to compute flows only from *b*=−90 to 90 degrees.

5. Computed Results

Two series of computations are performed, which are 1) four-seam case and two-seam case. Mizota et al.(1995) performed wind tunnel measurements in the four-seam case at the Reynolds number 1.0×10^5 and reported the aerodynamic coefficients at various angle *a*. Computed results are firstly compared with their measurements. All computations were done on a Fujitsu VPP500 with 28 processor elements at RIKEN, which is a vector-parallel computer whose theoretical peak performance is 44.8 GFLOPS. It took about 8 to 10 hours to calculate flows up to non-dimensional time 100 in the coarse grid case and 100 hours in the fine grid case. All aerodynamic forces and flow fields are taken averaged from non-dimensional time 20.0 up to 100.0. The code was parallelized and executed on 28 processor elements on the VPP500.

5.1 Four-seam Case

5.1.1 Aerodynamic coefficients

The shape of the seam has a period of 90 degrees in *a*-direction because of the geometrical symmetry. Calculated drag coefficients using the coarse grid system are plotted in Fig. 6 as the solid line, compared with the measurements (dotted lines). The experimental data were originally measured from *a*=0 to 360 degrees and are plotted as in between 0 and 90 degree. Computed results qualitatively show good agreement with the experiments although the values are about 20 percent lower than the measured values. Points A and B in the Fig. 6 show the computed drag coefficients using the fine grid system. Although the grid density increases from the coarse grid system, it dose not improve the gap.

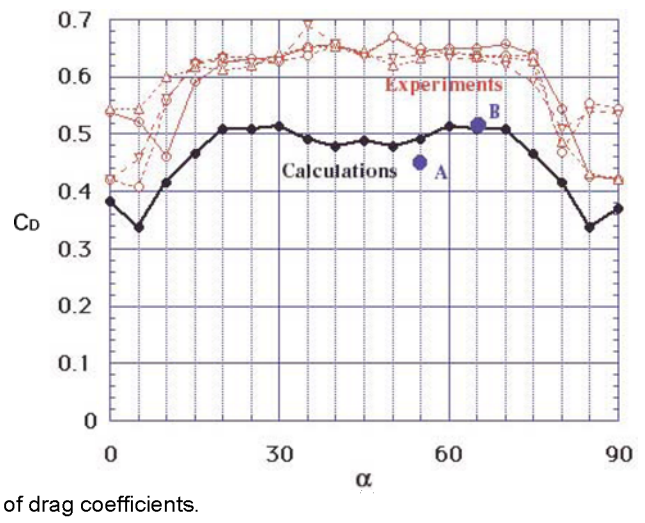

Fig. 6. Comparison of drag coefficients.

Figure 7 shows the calculated side force coefficients compared with the experimental data. The side force measured in experiments has sharp transition near *a*=45 degrees although the calculated force have only gradual change there. The calculated forces are about half in value. However, the experiments show that the transition point is not fixed and varies from 30 to 60 degrees. It becomes slower transition when those values are taken averaged. The results for the finer grid calculations are shown in Fig. 7 as point A and B. In this case, discrepancy

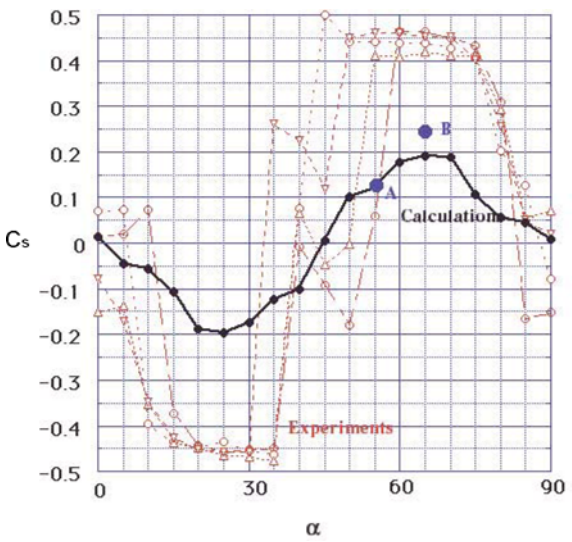

Fig. 7. Comparison of side coefficients.

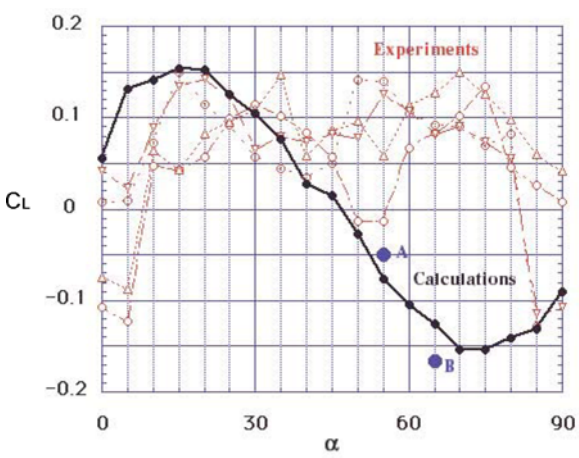

Fig. 8. Comparison of lift coefficients.

decreases at B as the grid density goes up.

Figure 8 shows the calculated lift coefficients as the solid lines compared with the experimental data plotted as the dotted lines. The calculated values themselves are not much different but the characteristics of the curve are totally different. Because of the geometric symmetry of the shapes shown in Fig. 4, the curve of lift coefficient variation should be the point symmetric with respect to *a*=45 degrees. The calculated results clearly show point symmetry but the measured values do not. This would be caused by a supporting rod that suspends the ball at the

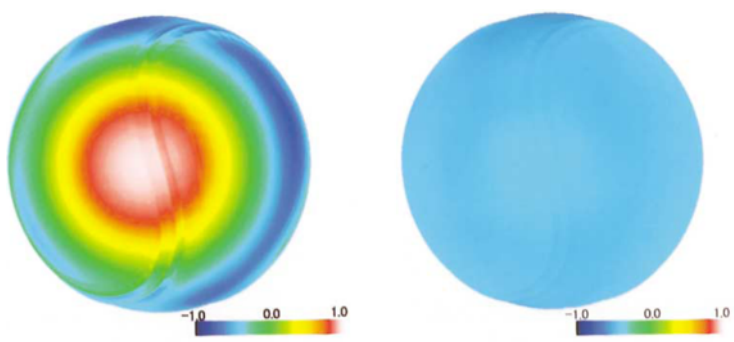

(a) front view (b) rear view

Fig. 9. Surface static pressure distribution: *a*=45 degrees.

bottom in the wind tunnel.

Finer grid results are also plotted in Fig. 8 as points A and B, and B shows larger negative values than those of the coarse grids.

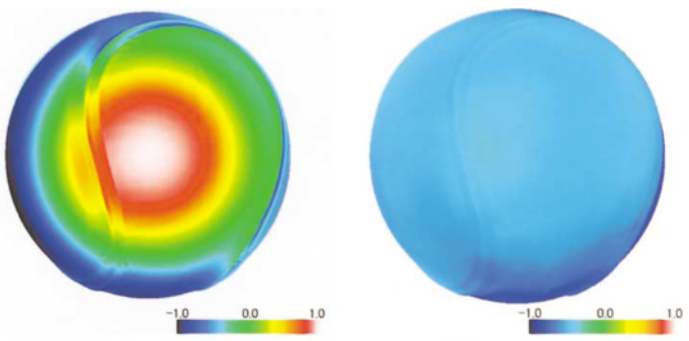

Fig. 10. Surface static pressure distribution: *a*=65 degrees.

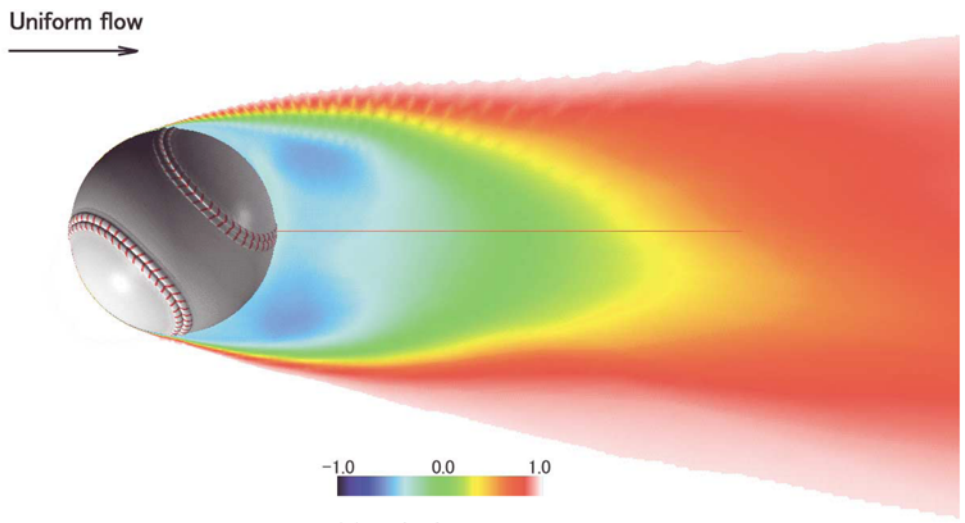

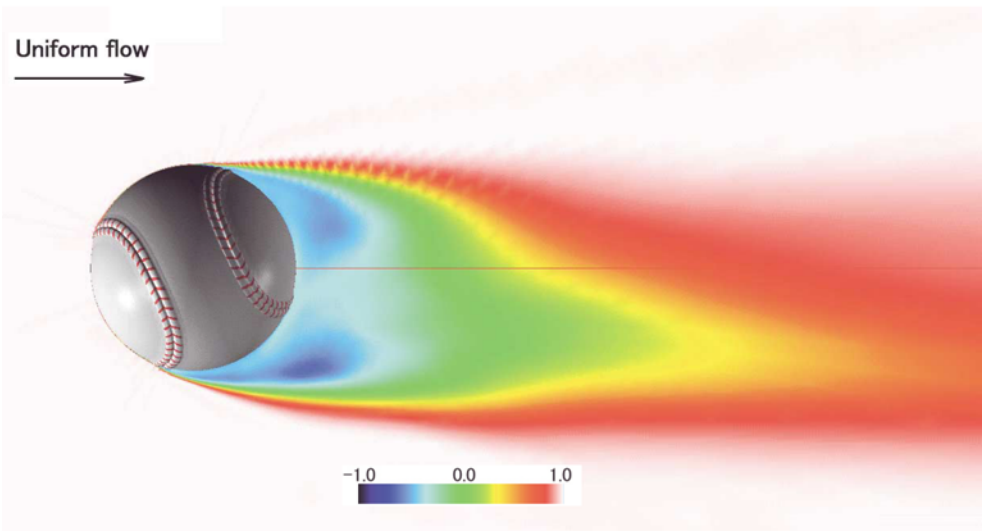

Fig. 11. Time-averaged total pressure distributions.

5.1.2 Flow fields

As shown in Fig. 7, large asymmetric force acts on the ball around a=60 degrees. The largest side force is observed at a=65 degrees and nearly no side force acts at a=45 degrees. Figures 9 and 10 show the front and rear views of time-averaged static pressure distributions on the ball surface at a=45 and 65 degrees respectively. The pressure distribution at a=45 degrees in Fig. 9(a) is almost symmetric and Figure 9(b) shows that there is little pressure difference on the rear half surface. The slight asymmetrical pressure distributions in the front half surface generates C_S: 0.006 in this case. On the other hand, pressure distributions at a=65 degrees in Fig. 10 are much more asymmetrical than the case of a=45 and the peak negative pressure is much higher. C_S in this case is 0.192.

Mizota et al.(1995) reported that the wake of a ball is slanted when the side force is acting and that the wake

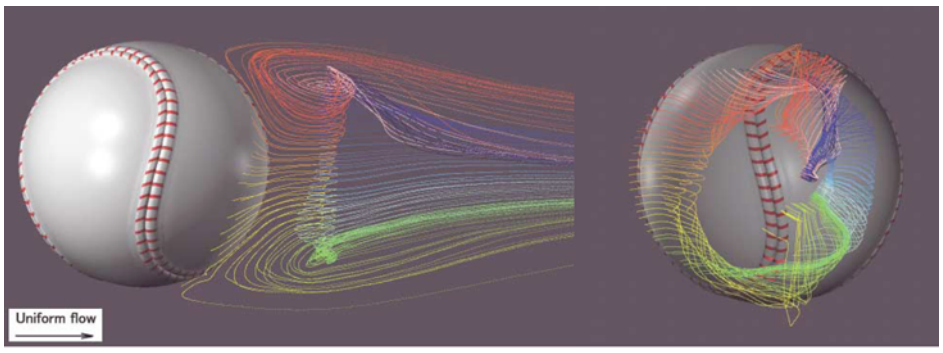

(a) side view (b) rear view

Fig. 12. Streamline in the wake at a=45 degrees.

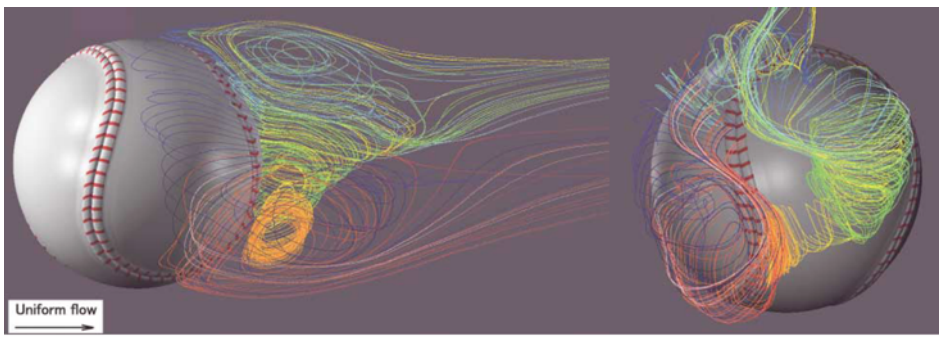

(a) side view (b) rear view

Fig. 13. Streamline in the wake at a=65 degrees.

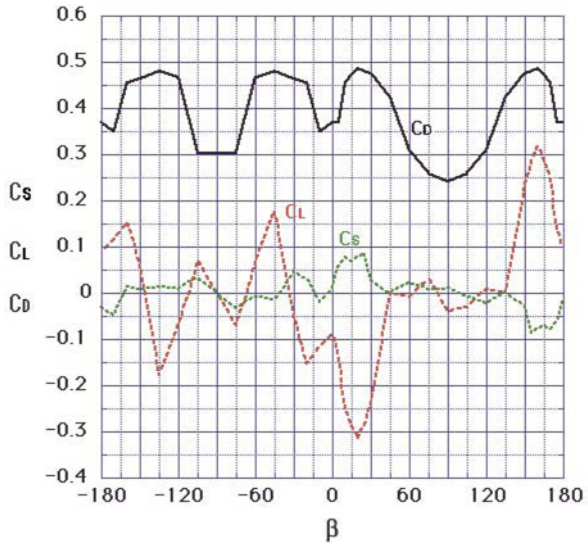

Fig. 14. Aerodynamic coefficient variations in two-seam cases.

is symmetric at a=45 degrees. To validate the computed results, time-averaged total pressure distributions at a=45 and a=65 degrees are compared with each other in Fig. 11. The horizontal red lines in Fig. 11 show lines of symmetry to see how much the wake is slanted. The computed wake at a=45 degrees is little slanted downward but the wake at a=65 apparently shifts downward.

Figures 12 and 13 show the streamline in the wake at a=45 and a=65 degrees respectively. A vortex ring and a pair of weak longitudinal vortices are found in the wake at a=45 degrees. At a=65 degrees, the ring vortex disappears and the longitudinal vortices increase their strength. The slanted wake and the side force are caused by these longitudinal vortices.

5.2 Two-seam Case

5.2.1 Aerodynamic coefficients

Aerodynamic coefficients are calculated and plotted in Fig. 12 from b=−75 to 90 degrees. The drag coefficient at b=90 degrees is 0.243 and is the lowest not only in b variation but also in a variation. The largest drag coefficient is observed at b=30, 60 degrees and is 0.514 which is more than twice of the lowest value: 0.243 at b=90 degrees. The largest lift force is observed at b=20 degrees and its value is −0.316. This absolute value is the largest asymmetric force among Figs. 7, 8 and 14. In other words, this is the largest force perpendicular to the uniform flow among all the calculated cases.

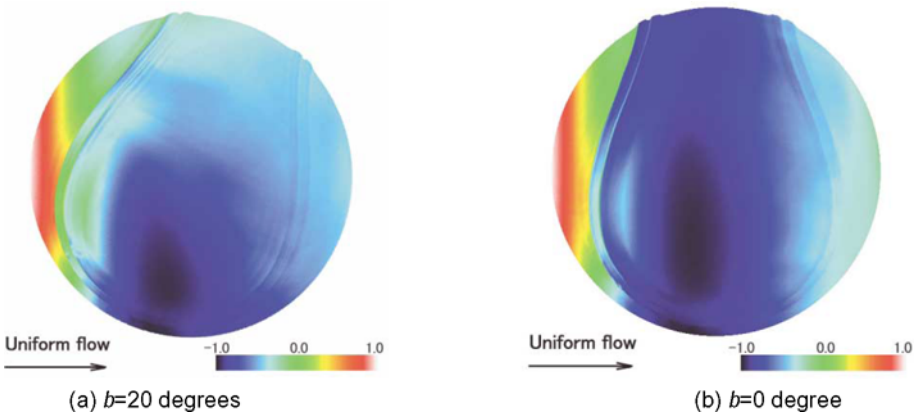

Fig. 15. Surface pressure distributions at b=20 and 0 degree.

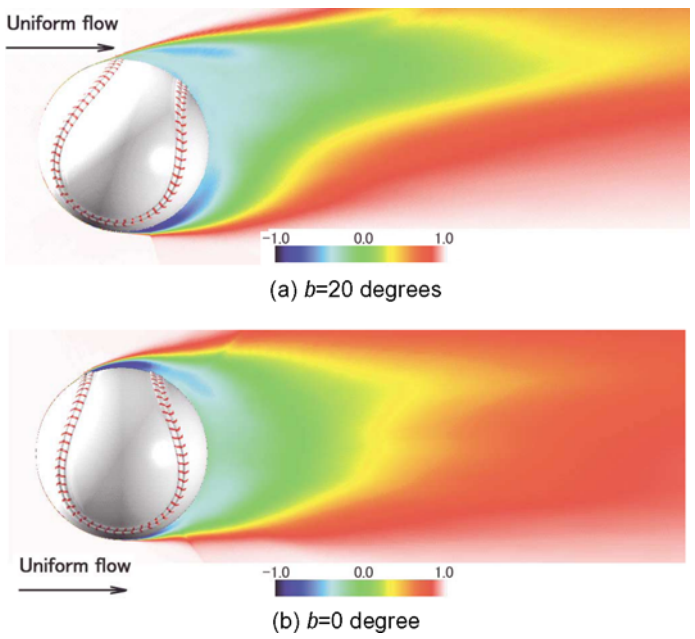

Fig. 16. Total pressure distributions at b=20 and 0 degree.

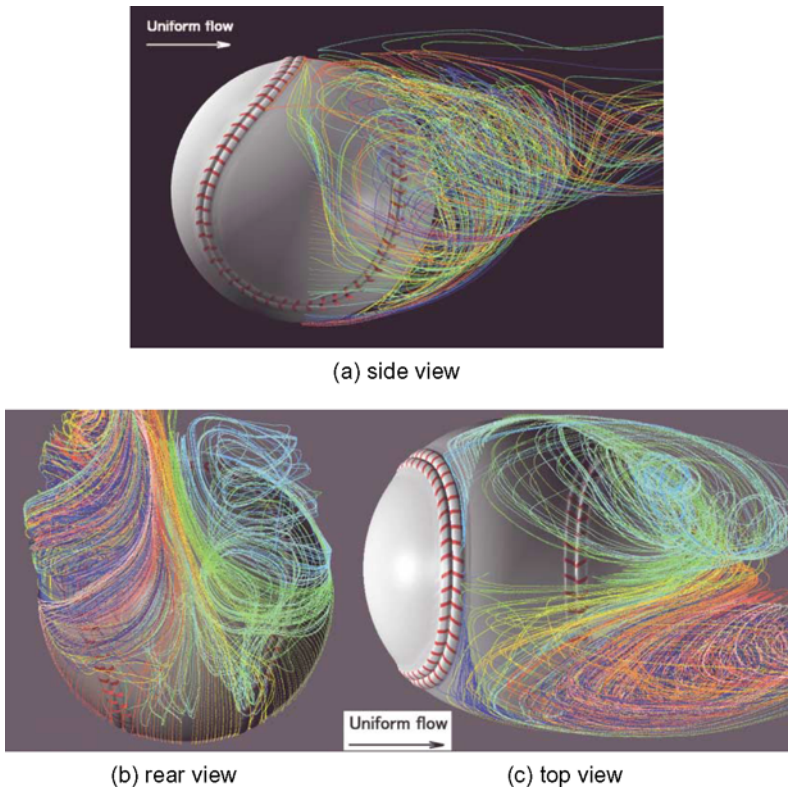

Fig. 17. Streamline in the wake at b=20 degrees.

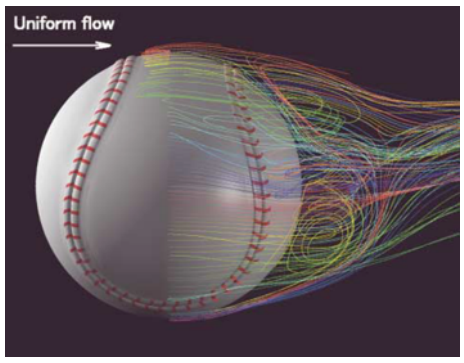

Fig. 18. Streamline in the wake at b=5 degrees.

5.2.2 Flow fields

In order to investigate why the lift coefficient at b=20 degrees is so high, the flow fields at b=20 degrees are compared with other cases. Figure 15 shows the side view of the time-averaged surface pressure distributions at b=20 degrees compared with b=0 degree. Main difference appears at the top of the ball. The projection of the seam at b=20 degrees causes large separation at the top and makes the pressure higher. This is more clearly shown in Fig. 16 that shows the total pressure distributions at b=20 and 0 degree. At b=20 degrees, the wake is strongly shifted upward. Figure 17 shows streamlines at b=20 degrees, which clearly shows a pair of longitudinal vortices in the wake. The longitudinal vortices have counter rotation with each other and generate lift force on the ball like an airplane. At the same time, the vortices make the wake slanted. When the separation at the top is not so large, a vortex ring appears instead of longitudinal vortices as shown in Fig. 18.

6. Conclusions

Flows around a ball with a seam line used in a baseball game are numerically simulated in two kinds of rotation. Those are four-seam rotation with an angle: a and two-seam rotation with an angle: b. The computed results of the four-seam rotation are compared with experimental data measured in a wind tunnel. The computed drag

coefficients qualitatively agree well with experiments. However, lift coefficients do not agree well. The computed results and geometrical symmetry suggest that a supporting rod at the bottom of the ball in the wind tunnel causes errors in measuring lift force. It is also observed in the computed results that wake is periodically changing from symmetric shape to slant shape as a increases. Present computation method is validated by these facts. When the wake is slanted, a pair of strong vortices are observed in the wake.

Flow changes in two-seam rotation are also simulated. It is found that the lowest drag force is observed at b=90 and the value is less than half of the largest drag force at a=30 and 60 degrees. The largest lift force is observed at b=20 degrees. In this case, a projection of the seam line on the top causes a large separation while smooth surface without the seam at the bottom dose not separate the flow. A pair of longitudinal vortices are found in the wake, which make wake slant and generate large lift force. When wake is nearly symmetric, a ring vortex is observed instead of a pair of longitudinal vortices..

Acknowledgment

The author would like to sincerely thank Mrs. Sanae Sato for her efforts on generating the grid system used in this study. The author also would like to express his thanks to Prof. Mizota for his kindness of offering his experimental data.

References

Himeno, R., Takagi, M., Fujitani, K. and Tanaka, H., Numerical Analysis of the Airflow around Automobiles Using Multi-block Structured Grids, SAE Paper 900319 (1990), The Society of Automotive Engineers.

Kawamura, T. and Kuwahara, K., Direct Simulation of a Turbulent Inner Flow by Finite Difference Method, AIAA paper, AIAA-85-0376 (1985).

Kawamura, T., Takami, H. and Kuwahara, K., Computation of High Reynolds Number Flow around a Circular Cylinder with Surface Roughness, Fluid Dynamic Research 1 (1986), 145-162.

Mehta, R. D., Aerodynamics of Sports Ball, Annual Review of Fluid Mechanics, 17 (1989), 151-189.

Mizota, T., Kuba, H. and Okajima, A., Erratic Behavior of Knuckle Ball (1) Quasi-steady Flutter Analysis and Experiment, Journal of Wind Engineering, No.62, January (1995), 3-13.

Mizota, T., Kuba, H. and Okajima, A., Erratic Behavior of Knuckle Ball (2) Wake Field and Aerodynamic Forces, Journal of Wind Engineering, No.62, January (1995), 15-22.

Ono, K., Himeno, R., Fujitani, K. and Uematsu, U., Simultaneous Computation of the External Flow around a Car Body and the Internal Flow through its Engine Compartment, SAE Paper 920342 (1992), The Society of Automotive Engineers.

Roache, P. J., Computational Fluid Dynamics, (1976), Hermora Publishers, New York.

Tani, I., Curve in a Baseball Game, Science Journal of Kagaku, 20-9 (1950), 405-409 (in Japanese).

Watts, R. G. and Sawyer, E., Aerodynamics of Knuckleball, American Journal of Physics, 43-11 (1975), 961-963.

Author Profile

Ryutaro Himeno: He received his B.E. and M.E. degrees in Electrical Engineering from Kyoto University, Kyoto, Japan in 1977 and 1979, respectively. He received Dr. Eng. in CFD from the University of Tokyo in 1988. From 1979 to 1997, he worked at Nissan Motor Co., Ltd., Yokosuka, Japan, where he engaged in the research of applying CFD to the car aerodynamics. From 1984 to 1986, he served as a researcher at the Institute of Space and Astronautical Science, Tokyo, Japan. In 1998, he joined RIKEN (The Institute of Physical and Chemical Research) and is Head of Computer and Information Division, Advance Computer and Information Center, RIKEN.